Mechanism of Néel Order Switching in Antiferromagnetic Thin Films Revealed by Magnetotransport and Direct Imaging

L. Baldrati,[1,*] O. Gomonay,[1] A. Ross,[1,2] M. Filianina,[1,2] R. Lebrun,[1] R. Ramos,[3] C. Leveille,[1] F. Fuhrmann,[1] T. R. Forrest,[4] F. Maccherozzi,[4] S. Valencia,[5] F. Kronast,[5] E. Saitoh,[3,6,7,8,9] J. Sinova,[1] and M. Kläui[1,2]

[1]*Institute of Physics, Johannes Gutenberg-University Mainz, 55128 Mainz, Germany*
[2]*Graduate School of Excellence Materials Science in Mainz, 55128 Mainz, Germany*
[3]*WPI-Advanced Institute for Materials Research, Tohoku University, Sendai 980-8577, Japan*
[4]*Diamond Light Source, Chilton, Didcot, Oxfordshire OX11 0DE, United Kingdom*
[5]*Helmholtz-Zentrum Berlin für Materialien und Energie, Albert-Einstein-Strasse 15, D-12489 Berlin, Germany*
[6]*Institute for Materials Research, Tohoku University, Sendai 980-8577, Japan*
[7]*Advanced Science Research Center, Japan Atomic Energy Agency, Tokai 319-1195, Japan*
[8]*Center for Spintronics Research Network, Tohoku University, Sendai 980-8577, Japan*
[9]*Department of Applied Physics, The University of Tokyo, Tokyo 113-8656, Japan*

(Received 26 October 2018; revised manuscript received 7 August 2019; published 24 October 2019)

We probe the current-induced magnetic switching of insulating antiferromagnet–heavy-metal systems, by electrical spin Hall magnetoresistance measurements and direct imaging, identifying a reversal occurring by domain wall (DW) motion. We observe switching of more than one-third of the antiferromagnetic domains by the application of current pulses. Our data reveal two different magnetic switching mechanisms leading together to an efficient switching, namely, the spin-current induced effective magnetic anisotropy variation and the action of the spin torque on the DWs.

DOI: 10.1103/PhysRevLett.123.177201

Electrical readout and writing of the antiferromagnetic state is crucial to exploit the properties of antiferromagnets in future spintronic devices. Antiferromagnetic materials have the potential for ultrafast operation [1], with spin dynamics in the terahertz range, high packing density, due to the absence of stray magnetic fields, and an insensitivity to magnetic fields [2,3]. Furthermore, low-power operation is possible in antiferromagnetic insulators (AFM-Is) due to long spin diffusion lengths [4] and the theoretical prediction of superfluid spin transport [5].

Recently, the electrical reading of the Néel order ($\mathbf{n}$) orientation in AFM-Is was demonstrated via spin Hall magnetoresistance (SMR) [6–10], a magnetoresistive effect depending on the mutual orientation of the magnetic order and an interfacial spin accumulation $\boldsymbol{\mu}_s$. However, one of the main challenges faced by AFM spintronics is the reliable electrical writing of the orientation of $\mathbf{n}$. One possible approach exploits staggered Néel spin orbit torques [11], creating an effective field of opposite sign on each magnetic sublattice. However, these torques rely on special material requirements, which has limited their application to the conducting AFMs CuMnAs and Mn_2Au [12–16]. Another approach would be to use the nonstaggered, anti-damping-like torque exerted by a spin accumulation at the interface of a heavy metal and an AFM-I. A charge current in the heavy metal layer can generate a transverse spin current via the spin Hall effect, creating anti-damping-like torques in the antiferromagnet. The possibility of such switching was demonstrated in NiO(001)/Pt and Pt/NiO(111)/Pt [17,18], but the mechanisms are still debated. One of the possible mechanisms relies on spin-current induced domain wall (DW) motion [19], predicting that DWs with opposite chirality are driven in opposite directions, thus excluding the electrical signature of the switching when DWs with opposite chirality are equally probable. A second mechanism [18], based on the coherent rotation of $\mathbf{n}$, predicts a current threshold 10 times larger than that found experimentally. A third mechanism, based on fieldlike torques acting on uncompensated interfacial spins, requires perfectly flat interfaces [17]. Currently, none of these provides a consistent explanation of the effect.

In this work we realize reliable current-induced switching in epitaxial antiferromagnetic NiO/Pt bilayers. We show that the magnetic state of the NiO can be switched up to a thickness of at least 90 nm. By direct imaging of the current-induced switching, we single out the role of AFM DWs. Two switching mechanisms are identified to be involved, either breaking the degeneracy of $\mathbf{n}$ with respect to the spin accumulation $\boldsymbol{\mu}_s$ or not. We attribute the degeneracy-breaking mechanism to a ponderomotive force, created by the anti-damping-like torque, which displaces the DWs and favors domains with $\mathbf{n} \perp \boldsymbol{\mu}_s$. A second non-degeneracy-breaking switching mechanism stems from the torque directly acting on the DWs, locally inducing switching in different directions ($\mathbf{n} \| \boldsymbol{\mu}_s$, $\mathbf{n} \perp \boldsymbol{\mu}_s$). These two

mechanisms occur in AFMs with depinning fields of the DWs lower than the anisotropy fields, which is the case in NiO and most AFM-Is [9,10].

To study switching in AFM-Is, we grew epitaxial NiO(001)/Pt bilayers [20]. The magnetic properties were checked by the polarization-dependent absorption spectrum around the Ni L_2 edge [Fig. 1(a)], which shows x-ray magnetic linear dichroism (XMLD) and no circular dichroism (XMCD) [10,32,33], a signature of antiferromagnetic ordering. We read electrically the orientation of $\mathbf{n}$ by the SMR, since the transverse resistance of a heavy metal/AFM-I bilayer depends on the product $n_x{}^* n_y$ [10]. To apply current pulses and measure the SMR, micrometric Hall cross devices were lithographically patterned and etched by Ar ions. For the SMR measurements, we applied a probing current density $j \sim 10^9$ A m^{-2} and the relative transverse resistance variation was calculated as $[(\Delta R_{\mathrm{transv}})/\bar{R}] = \{[V(I^+) - V(I^-)]/(\bar{R}I)\}$, where $\bar{R}$ is the average longitudinal resistance, V is the transverse voltage [Fig. 1(b)], and I is the current, whose sign is reversed to eliminate thermal effect contributions. We applied current pulses and performed the measurements 10 s later, to probe equilibrium conditions.

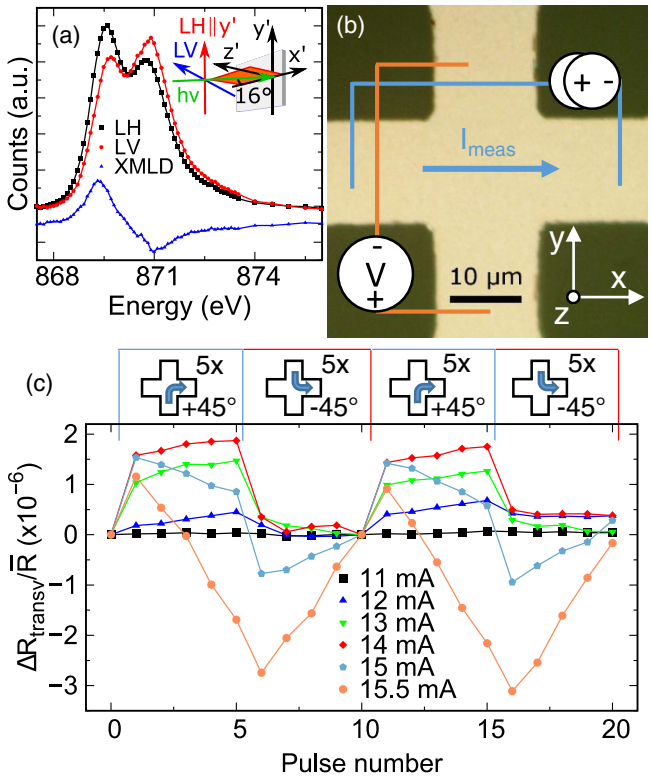

FIG. 1. (a) X-ray absorption spectrum at the Ni L_2 edge for linearly vertical (LV) and horizontal (LH) polarized light of MgO(001)//NiO(25 nm)/Pt(2). (b) Optical micrograph of a device and contact scheme used for the transverse resistance measurements. (c) Electrical switching of the transverse resistance in a MgO(001)//NiO(5 nm)/Pt(2 nm) sample. The pulse pathway is changed every 5 pulses as indicated.

The switching characteristics of an 8 μm wide Hall cross device on a MgO(001)//NiO(001)(5 nm)/Pt(2 nm) sample, obtained by changing the direction of the 1-ms long current pulses by 90° every five pulses is shown in Fig. 1(c) (a linear background was subtracted [20]). At 13 mA ($j = 8.1 \times 10^{11}$ Am^{-2}), the normalized transverse resistivity variation increases (decreases) after the application of current pulses along a direction at +45° (−45°) with respect to the measurement current direction. The first +45° pulse induces a "steplike" increase of the transverse resistance signal. The signal amplitude increases slightly with the following 4 pulses of the same orientation, with a tendency to saturate. At 15 mA +45° ($j = 9.4 \times 10^{11}$ A m^{-2}), the transverse resistance again increases abruptly as for smaller currents. However, the signal decreases after the following pulses, implying a reversed sign of the switching and thus indicating the presence of at least two competing mechanisms contributing to the measured electrical signal. At even higher current densities only a "triangularlike" behavior is seen. In Ref. [20] we show that the "triangularlike" behavior at high currents is a thermal effect related to the Pt, observed also in MgO/Pt and in NiO/Pt with Pt grown *ex situ*. The transverse resistance variation likely stems from the current-induced annealing and electromigration of the Pt deposited at room temperature, that locally changes the resistivity and yields different current paths in the system. On the other hand, we observed the "steplike" switching only in NiO/Pt with Pt grown *in situ*, suggesting that this is related to the spin transport across the NiO/Pt interface and thus to the SMR probing the magnetic order in the NiO. While the switching depends on the pulse current orientation, it does not significantly depend on the polarity. The sign of the switching is consistent with the readout by spin Hall magnetoresistance of a final state $\mathbf{n} \| \boldsymbol{j}$ [7,10], implying that the degeneracy between the $\mathbf{n} \perp \boldsymbol{\mu}_s$ and $\mathbf{n} \| \boldsymbol{\mu}_s$ configurations is broken. In Ref. [18], this switching was attributed to a spin-current induced anti-damping-like torque acting in strained biaxial NiO(001), according to a macrospin model. However, the multilevel final state of the switching in contrast suggests that the switching comprises the redistribution of antiferromagnetic domains or effects related to the Pt.

To develop a theory consistent with the experimental results, we first consider mechanisms based on the motion of AFM DWs. We start by the spin-current-induced dynamics of a simple antiferromagnetic texture comprising of two regions with a homogeneous direction of the Néel order, the domains A and B. These are separated by a DW, as shown schematically in Fig. 2. The orientation of $\mathbf{n}$ in two contiguous NiO domains can vary by different angles, due to the complex anisotropy of the material. We here consider 90° domains that are instructive to explain our model but the physical mechanism is not limited to this situation. The translational motion of the DW has the lowest activation energy (zero in the absence of pinning)

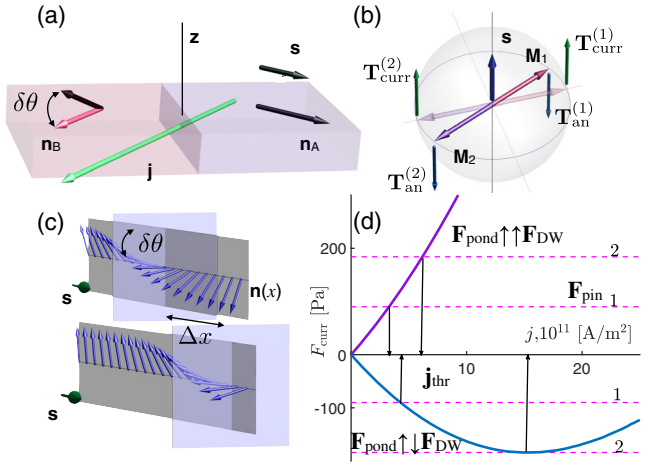

FIG. 2. (a) A current with density $\boldsymbol{j}\perp\mathbf{n}_A$ injects a spin current with polarization $\boldsymbol{s}\propto(\boldsymbol{j}\times\hat{\boldsymbol{z}})\|\mathbf{n}_A$, creating a torque $\mathbf{T}_{\rm curr}$. The torque rotates $\mathbf{n}_B$, initially $\|\boldsymbol{j}$, by an angle $\delta\theta$, but does not affect $\mathbf{n}_A$. (b) Because of the SOTs, $\mathbf{M}_{1,2}$ rotates from the easy axis (semitransparent arrows) toward the new equilibrium state (opaque arrows) where $\mathbf{T}_{\rm curr}^{(1,2)}$ are compensated by the anisotropy torques $\mathbf{T}_{\rm an}^{(1,2)}$. (c) The SOT-induced translation of the DW by a distance Δx is equivalent to the rotation of $\mathbf{n}$ inside the DW region by an angle $\delta\theta$. (d) Current dependence of $\mathbf{F}_{\rm curr}$, when $\mathbf{s}$ is almost parallel to the easy plane (deflection 5°). The force pushes the DWs toward the unfavorite domain ($\mathbf{F}_{\rm pond}\uparrow\uparrow\mathbf{F}_{\rm DW}$), but for low current density and low pinning force (dashed line 1) the DW is pushed toward the favorite one ($\mathbf{F}_{\rm pond}\uparrow\downarrow\mathbf{F}_{\rm DW}$). A large pinning force (dashed line 2) blocks the DW motion.

among all possible types of magnetic excitations and can be considered as the main mechanism of spin-current induced dynamics in AFMs with nonzero anisotropy like NiO [9,10]. In this case, the DW dynamics follows the equation of a point mass with momentum $\mathbf{P}$ [34]: $[(d\mathbf{P})/(dt)]=-\gamma_d\mathbf{P}+\mathbf{F}_{\rm curr}+\mathbf{F}_{\rm pin}$, where γ_d is the effective damping, $\mathbf{F}_{\rm pin}$ is a pinning force, and $\mathbf{F}_{\rm curr}$ is the force induced by the current, which is comprised of two components, as described below.

A charge current with a density $\boldsymbol{j}$ flowing in the Pt layer generates a dampinglike spin-orbit torque (SOT) $\mathbf{T}_{\rm curr}=\hbar\varepsilon\theta_H\mathbf{n}\times(\boldsymbol{j}\times\hat{\boldsymbol{z}})\times\mathbf{n}/(2ed_{\rm AFM}\boldsymbol{M}_s^2)$, acting on $\mathbf{n}$. Here $\hbar$ is the Planck constant, $d_{\rm AFM}$ is the thickness of the active layer of the antiferromagnet, $0<\varepsilon\leq 1$ is the spin-polarization efficiency, θ_H is the spin Hall angle, e is the electron charge, and $M_s=|\boldsymbol{n}|$. In a homogeneous state, this torque competes with that $\mathbf{T}_{\rm an}=\mathbf{n}\times\mathbf{H}_{\rm an}$ created by the magnetic anisotropy field $\mathbf{H}_{\rm an}$, and can rotate $\mathbf{n}$ from an easy axis towards a new equilibrium direction $\mathbf{n}+\Delta\mathbf{n}$ [Figs. 2(a),2(b)]. The virtual work produced by the SOT in such static rotation is associated with the potential energy density $U_{\rm curr}=\hbar\varepsilon\theta_H(\hat{\boldsymbol{z}}\times\boldsymbol{j})\cdot(\mathbf{n}\times\Delta\mathbf{n})/(2ed_{\rm AFM}\boldsymbol{M}_s^2)$; i.e., the spin current acts like an additional magnetic anisotropy term which depends on $\mathbf{n}$: $U_{\rm ma}\rightarrow U\equiv U_{\rm ma}+U_{\rm curr}$ [20]. The resulting energy imbalance between the two domains entails a force which drives the DW into the energetically unfavorable domain. We call this force due to its nature the ponderomotive force $F_{\rm pond}=U(\mathbf{n}_A)-U(\mathbf{n}_B)\propto(\boldsymbol{j}\cdot\mathbf{n}_B)^2-(\boldsymbol{j}\cdot\mathbf{n}_A)^2$. In a multidomain sample, $\mathbf{F}_{\rm pond}$ breaks the degeneracy of the domains with different $\mathbf{n}$ and thus induces switching toward a state with $\mathbf{n}\perp\boldsymbol{\mu}_s$, as we observe here experimentally. Note that the thermally activated processes in our theory can be modelled as a temperature dependent pinning force $\mathbf{F}_{\rm pin}$, which decreases with increasing temperature.

To further investigate the role that the antiferromagnetic domains and DWs play in the switching mechanism, we performed XMLD-photoemission electron microscopy (PEEM) imaging of the NiO domains in NiO(001) samples [33], grown at the same time as the ones for electrical measurements, while applying *in situ* current pulses. The imaging was performed using a two energy mode at the Ni L_2 double peak [32], using linearly polarized x rays with the electric field out of the plane of the sample [Fig. 1(a) and Ref. [20]], yielding sensitivity to components of $\mathbf{n}$ parallel or orthogonal.

We show in Figs. 3(a)–3(i) the domain structure of a MgO//NiO(10 nm)/Pt(2 nm) sample, before and after the application of pulses across two orthogonal arms of a

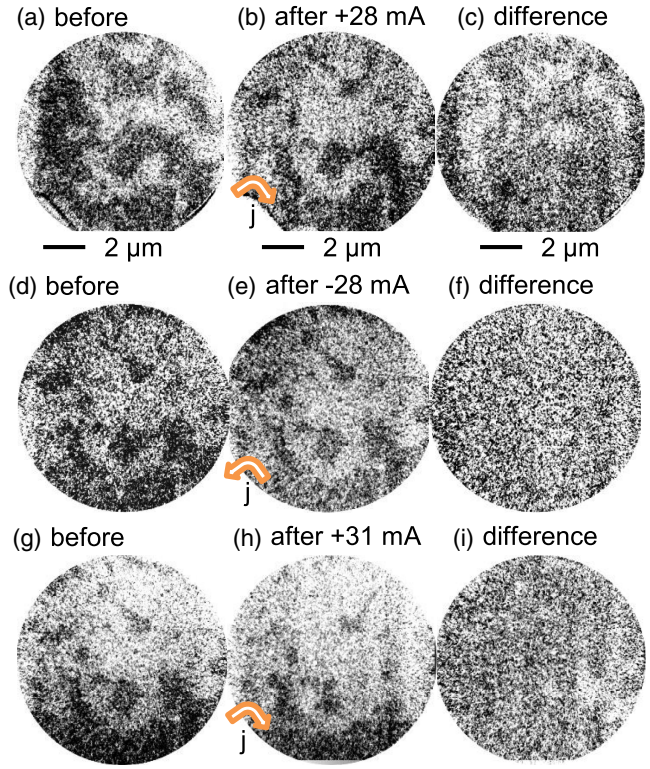

FIG. 3. Switching of antiferromagnetic domains in MgO// NiO(10)/Pt(2), imaged with out-of-plane x-ray polarization. Three sequences of images before and after 5 pulses 1 ms long are shown together with the difference image. The direction of the current density j is shown by the arrows in panels (b),(e),(h).

Hall cross, as measured at the SPEEM end station at Helmholtz-Zentrum Berlin [35]. We applied sequences of 5 pulses 1 ms long with currents of +28 [Figs. 3(a)–3(c), $j = 1.4 \times 10^{12}$ Am^{-2}], −28 [Figs. 3(d)–3(f)], and +31 mA [Figs. 3(g)–3(i), $j = 1.5 \times 10^{12}$ Am^{-2}]. We first note that, after the application of the +28 mA pulse train, the contrast changes in approximately one-third of the area, towards more white contrast [Figs. 3(a)–3(c)]. Given the formula used to calculate the contrast [20], the final state has increased areas with $\mathbf{n}$ out of the plane of the sample (parallel to the x-ray polarization), consistent with our model predicting a final state with $\mathbf{n} \perp \boldsymbol{\mu}_s$. Moreover, a large domain area goes instead toward more black (in-plane). We cannot resolve in-plane components of $\mathbf{n}$ with this measurement configuration, but there is an in-plane direction with $\mathbf{n} \perp \boldsymbol{\mu}_s$. Pulses with current lower than 28 mA did not change the domain structure significantly. One can see that some domains shrink after the pulse train, while other domain walls do not move, as described in our model by the space dependent pinning force. Reversing the current sign and applying 5 additional current pulses [Figs. 3(d)–3(f)] yields again more white domains, consistently with the independence on the pulse current polarity and the tendency to saturate found in electrical measurements. Finally, at even larger current density [Figs. 3(g)–3(i)] we observe additional switching toward more out-of-plane domains, showing that the switching is deterministic and increases with increasing current density, in line with our model.

In addition to this unidirectional deterministic switching, further switching mechanisms have been predicted that change the domain structure but keep the average distribution of $\mathbf{n}$ constant, so they cannot be detected by electrical means. To check if this is the case, we imaged the domain structure of a MgO//NiO(25 nm)/Pt(2 nm) sample with in-plane x-ray polarization, before and after the application of 1000 current pulses 10 μs long with a lower current density of 7.5×10^{11} Am^{-2}, where no significant switching is detected electrically. Such a switching event is shown in Figs. 4(a)–4(c), together with the difference image, as measured at the beam line I06 of the Diamond light source. One can see sub-μm sized antiferromagnetic domains switching after the application of the pulses. In particular, we observe switching having in-plane components in both directions ($\mathbf{n} \| \boldsymbol{\mu}_s$, $\mathbf{n} \perp \boldsymbol{\mu}_s$) for a single pulse direction. To check for pure thermal effects, we imaged previously the domain structure as a function of temperature and did not observe pure thermal switching of the antiferromagnetic domains [10], implying that the switching observed here is current induced due to generated torques. The switching mechanism observed here, not breaking the degeneracy between the ($\mathbf{n} \| \boldsymbol{\mu}_s$, $\mathbf{n} \perp \boldsymbol{\mu}_s$) states, is not explained by the anti-damping-torque theory [18], and it is not consistent with the symmetry of the pondermotive force, thus calling for an additional theoretical explanation. For this second switching mechanism, in

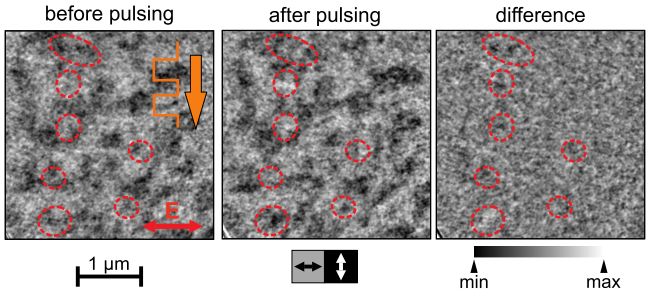

FIG. 4. Switching of antiferromagnetic domains in MgO// NiO(25)/Pt(2) imaged with in-plane x-ray polarization. The NiO domain structure is shown (a) before and (b) after the application of 1000 pulses 10 μs long, with a current density of 7.5×10^{11} Am^{-2}. (c) Difference between the images in panels (a),(b). Switching areas, showing different final states ($\boldsymbol{n} \| \boldsymbol{j}$, $\boldsymbol{n} \perp \boldsymbol{j}$) are encircled.

analogy to ferromagnets [36], we identify the SOT acting in inhomogeneous regions of the antiferromagnetic texture and inducing a coherent rotation of the spatially distributed $\mathbf{n}$, i.e., leading to translational DW motion [Fig. 3(c)] induced by a force $\mathbf{F}_{\mathrm{DW}}$. This force [19], (see derivation in Ref. [20])

$$\mathbf{F}_{\mathrm{DW}} = \frac{\hbar \varepsilon \theta_H}{2 e d_{\mathrm{AFM}} M_s^2} \int (\hat{\boldsymbol{z}} \times \boldsymbol{j}) \cdot (\mathbf{n} \times \nabla \mathbf{n}) dx, \qquad (1)$$

originates from the current-induced rotation of $\mathbf{n}$ within the DW (the DW dynamics induced by this force was considered in Ref. [19], but not the general expression considered here), is linear with the current and its direction depends only on the chirality of the DW ($\mathbf{n} \times \nabla \mathbf{n}$) and not on $\mathbf{n}_A$ and $\mathbf{n}_B$ inside the domains. $\mathbf{F}_{\mathrm{DW}}$, though able to locally induce fast motion of the DWs, does not globally break the degeneracy of the domains between the configurations ($\mathbf{n} \| \boldsymbol{\mu}_s$, $\mathbf{n} \perp \boldsymbol{\mu}_s$) once the DWs with opposite chirality are equiprobable, resulting in no electrical response. This is expected in cubic NiO, due to absence of interactions such as the Dzyaloshinskii-Moriya, breaking the chiral degeneracy.

Overall, both mechanisms identified from the combination of electrical measurements above the threshold and the imaging below the electrical threshold contribute to the switching. The current-induced force is thus $\mathbf{F}_{\mathrm{curr}} = \mathbf{F}_{\mathrm{pond}} + \mathbf{F}_{\mathrm{DW}}$. The resulting $\mathbf{F}_{\mathrm{curr}}$ acting on the DWs depends on the orientation of the current (spin polarization) with respect to the easy plane. If the current is almost parallel to the easy plane, $|\mathbf{F}_{\mathrm{DW}}| \sim |\mathbf{F}_{\mathrm{pond}}|$, the motion of the DWs into energetically favorable domains can be partially or fully blocked for one DW chirality, depending on the value of F_{pin} [Fig. 3(d)]. Note that $\mathbf{F}_{\mathrm{DW}}$, not breaking the degeneracy ($\mathbf{n} \| \boldsymbol{\mu}_s$, $\mathbf{n} \perp \boldsymbol{\mu}_s$), is not expected to lead to an electrical signal. This is distinctly different from the mechanism proposed in Ref. [17] for Pt/NiO(111)/Pt

trilayers, based on the fieldlike torque acting on the uncompensated spins at the interface, which are unlikely to form in our nonperfectly flat devices.

In the case of a pronounced angle between the easy plane and the film plane, as we have in NiO(001), the system exhibits $|\mathbf{F}_{DW}| > |\mathbf{F}_{pond}|$ at low current densities, and local switching in both directions (A to B or B to A) is possible. This is consistent with the direct observation by XMLD-PEEM of switching into different final states ($\mathbf{n}\|\boldsymbol{\mu}_s$ and $\mathbf{n}\perp\boldsymbol{\mu}_s$) at 7.5×10^{11} Am^{-2} in NiO(001). However, at higher current densities $\mathbf{F}_{pond} \propto I^2$ prevails over $\mathbf{F}_{DW} \propto I$, as shown in Fig. 2(d), and drives the deterministic switching as we see in Fig. 3. Antiferromagnetic DW motion induced by thermal gradients might also aid the switching process and lead to additional final states ($\mathbf{n}\|\boldsymbol{\mu}_s$, $\mathbf{n}\perp\boldsymbol{\mu}_s$) [37,38].

We finally compare the "steplike" switching in MgO(001)//NiO(d)/Pt(2 nm) samples, where $d = 5$, 90 nm (see Ref. [20]). The switching amplitude is larger and the maximum of the switching occurs at lower current densities for $d = 5$ nm. The easier switching in the thinner NiO layer can be explained by the reduced volume to be switched and by the smaller domains we observe in thicker NiO (see Ref. [20]), which indicate a higher density of pinning defects. Moreover, we can switch the NiO(001) up to a thickness of 90 nm, far beyond the highest spin-orbit torque switchable thickness reported in ferromagnetic $Tm_3Fe_5O_{12}$(8 nm)/Pt [39]. This allows us to speculate that the switching in NiO occurs in the interfacial region close to the Pt layer; i.e., the formation of surface domains in antiferromagnets is easier than in ferromagnetic systems, due to stronger destressing effects and the presence of dislocations at the surface [40]. These surface domains can be as small as the effective spin diffusion length of the NiO [41], of the order of few nm [42], i.e., the depths probed by the transverse SMR and XMLD-PEEM measurements.

To conclude, we demonstrated current-induced switching of the Néel order in the NiO/Pt system, revealing the origin of the switching. The switching comprises the redistribution of antiferromagnetic domains via domain wall motion, as probed both by electrical measurements and direct magnetic imaging, and occurs via two different mechanisms: one mechanism breaks the degeneracy of the domains ($\mathbf{n}\|\boldsymbol{\mu}_s$, $\mathbf{n}\perp\boldsymbol{\mu}_s$) and stems from the action of the spin current, which modifies the effective magnetic anisotropy, determining a ponderomotive force on the domain walls that leads to the switching detected by the electrical measurements above a threshold. The second mechanism stems from the direct action of the anti-damping-spin torque on the domain walls and does not break the degeneracy ($\mathbf{n}\|\boldsymbol{\mu}_s$, $\mathbf{n}\perp\boldsymbol{\mu}_s$) if domain walls with different chirality are equally probable, as identified from imaging below the electrical threshold. Our model has the potential to explain switching in antiferromagnetic systems in which anti-damping-like spin torques can be created, thus paving the way to the control of the switching necessary to enable future applications of AFMs in devices.

The authors thank J. Cramer, M. Asa, J. Henrizi, A. Dion, and T. Reimer for skillful technical assistance. We acknowledge useful scientific discussion with M. Jourdan. O. G. and J. S. acknowledge the support from the Humboldt Foundation, the ERC Synergy Grant SC2 (No. 610115), the EU FET Open RIA Grant no. 766566, the DFG (project SHARP 397322108), from the Ministry of Education of the Czech Republic Grant No. LM2015087 and LNSM-LNSpin. L. B., R. L., A. R., M. F., and M. K. acknowledge support from the Graduate School of Excellence Materials Science in Mainz (MAINZ) GSC 266, the DAAD (Spintronics network, Project No. 57334897) and all groups from Mainz acknowledge SFB TRR 173 Spin+X, in particular projects A01 and A03. L.B and R. L. acknowledge the European Union's Horizon 2020 research and innovation program under the Marie Skłodowska-Curie grant agreements ARTES No. 793159 and FAST No. 752195. We acknowledge Diamond Light Source for time on beam line I06 under proposals SI18850 and SI20698. We thank H. Z. B. for the allocation of synchrotron radiation beamtime. The research leading to this result has been supported by the project CALIPSOplus under the Grant Agreement 730872 from the EU Framework Programme for Research and Innovation HORIZON 2020. This work was also supported by ERATO "Spin Quantum Rectification Project" (Grant No. JPMJER1402) from Japan Science and Technology Agency (JST) and the Grant-in-Aid for Scientific Research on Innovative Area, "Nano Spin Conversion Science" (Grant No. JP26103005) from JSPS KAKENHI, Japan.

Note added.—During the preparation of this revised manuscript, we became aware of related work by Gray *et al.* [43].

*lbaldrat@uni-mainz.de

[1] K. Olejník, T. Seifert, Z. Kašpar, V. Novák, P. Wadley, R. P. Campion, M. Baumgartner, P. Gambardella, P. Nemec, J. Wunderlich, J. Sinova, P. Kužel, M. Müller, T. Kampfrath, and T. Jungwirth, Sci. Adv. **4**, eaar3566 (2018).
[2] J. Železný, P. Wadley, K. Olejník, A. Hoffmann, and H. Ohno, Nat. Phys. **14**, 220 (2018).
[3] V. Baltz, A. Manchon, M. Tsoi, T. Moriyama, T. Ono, and Y. Tserkovnyak, Rev. Mod. Phys. **90**, 015005 (2018).
[4] R. Lebrun, A. Ross, S. A. Bender, A. Qaiumzadeh, L. Baldrati, J. Cramer, A. Brataas, R. A. Duine, and M. Kläui, Nature (London) **561**, 222 (2018).
[5] S. Takei, B. I. Halperin, A. Yacoby, and Y. Tserkovnyak, Phys. Rev. B **90**, 094408 (2014).
[6] H. Nakayama, M. Althammer, Y. T. Chen, K. Uchida, Y. Kajiwara, D. Kikuchi, T. Ohtani, S. Geprägs, M. Opel, S. Takahashi, R. Gross, G. E. W. Bauer, S. T. B. Goennenwein, and E. Saitoh, Phys. Rev. Lett. **110**, 206601 (2013).

[7] G. R. Hoogeboom, A. Aqeel, T. Kuschel, T. T. M. Palstra, and B. J. van Wees, Appl. Phys. Lett. **111**, 052409 (2017).
[8] D. Hou, Z. Qiu, J. Barker, K. Sato, K. Yamamoto, S. Vélez, J. M. Gomez-Perez, L. E. Hueso, F. Casanova, and E. Saitoh, Phys. Rev. Lett. **118**, 147202 (2017).
[9] J. Fischer, O. Gomonay, R. Schlitz, K. Ganzhorn, N. Vlietstra, M. Althammer, H. Huebl, M. Opel, R. Gross, S. T. B. Goennenwein, and S. Geprägs, Phys. Rev. B **97**, 014417 (2018).
[10] L. Baldrati, A. Ross, T. Niizeki, C. Schneider, R. Ramos, J. Cramer, O. Gomonay, M. Filianina, T. Savchenko, D. Heinze, A. Kleibert, E. Saitoh, J. Sinova, and M. Kläui, Phys. Rev. B **98**, 024422 (2018).
[11] J. Železný, H. Gao, K. Výborný, J. Zemen, J. Mašek, A. Manchon, J. Wunderlich, J. Sinova, and T. Jungwirth, Phys. Rev. Lett. **113**, 157201 (2014).
[12] P. Wadley *et al.*, Science **351**, 587 (2016).
[13] S. Y. Bodnar, L. Šmejkal, I. Turek, T. Jungwirth, O. Gomonay, J. Sinova, A. A. Sapozhnik, H. J. Elmers, M. Kläui, and M. Jourdan, Nat. Commun. **9**, 348 (2018).
[14] M. J. Grzybowski, P. Wadley, K. W. Edmonds, R. Beardsley, V. Hills, R. P. Campion, B. L. Gallagher, J. S. Chauhan, V. Novak, T. Jungwirth, F. Maccherozzi, and S. S. Dhesi, Phys. Rev. Lett. **118**, 057701 (2017).
[15] P. Wadley, S. Reimers, M. J. Grzybowski, C. Andrews, M. Wang, J. S. Chauhan, B. L. Gallagher, R. P. Campion, K. W. Edmonds, S. S. Dhesi, F. Maccherozzi, V. Novak, J. Wunderlich, and T. Jungwirth, Nat. Nanotechnol. **13**, 362 (2018).
[16] M. Meinert, D. Graulich, and T. Matalla-Wagner, Phys. Rev. Applied **9**, 064040 (2018).
[17] T. Moriyama, K. Oda, and T. Ono, Sci. Rep. **8**, 14167 (2018).
[18] X. Z. Chen, R. Zarzuela, J. Zhang, C. Song, X. F. Zhou, G. Y. Shi, F. Li, H. A. Zhou, W. J. Jiang, F. Pan, and Y. Tserkovnyak, Phys. Rev. Lett. **120**, 207204 (2018).
[19] T. Shiino, S.-H. Oh, P. M. Haney, S.-W. Lee, G. Go, B.-G. Park, and K.-J. Lee, Phys. Rev. Lett. **117**, 087203 (2016).
[20] See Supplemental Material at http://link.aps.org/supplemental/10.1103/PhysRevLett.123.177201 for the materials properties, additional switching measurements including control samples, and the derivation of the theoretical model. This material includes Refs. [21–31].
[21] L. C. Bartel and B. Morosin, Phys. Rev. B **3**, 1039 (1971).
[22] F. W. Lytle, J. Appl. Phys. **35**, 2212 (1964).
[23] E. Langenberg, E. Ferreiro-Vila, V. Leborán, A. O. Fumega, V. Pardo, and F. Rivadulla, APL Mater. **4**, 104815 (2016).
[24] A. van den Brink, G. Vermijs, A. Solignac, J. Koo, J. T. Kohlhepp, H. J. M. Swagten, and B. Koopmans, Nat. Commun. **7**, 10854 (2016).
[25] A. Manchon, I. M. Miron, T. Jungwirth, J. Sinova, J. Zelezny, A. Thiaville, K. Garello, and P. Gambardella, Rev. Mod. Phys. **91**, 035004 (2019).
[26] F. B. Lewis and N. H. Saunders, J. Phys. C **6**, 2525 (1973).
[27] M. T. Hutchings and E. J. Samuelsen, Phys. Rev. B **6**, 3447 (1972).
[28] A. Schrön, C. Rödl, and F. Bechstedt, Phys. Rev. B **86**, 115134 (2012).
[29] H. V. Gomonay and V. M. Loktev, Phys. Rev. B **81**, 144427 (2010).
[30] H. V. Gomonay, R. V. Kunitsyn, and V. M. Loktev, Phys. Rev. B **85**, 134446 (2012).
[31] T. Kampfrath, A. Sell, G. Klatt, A. Pashkin, S. Mährlein, T. Dekorsy, M. Wolf, M. Fiebig, A. Leitenstorfer, and R. Huber, Nat. Photonics **5**, 31 (2011).
[32] K. Arai, T. Okuda, A. Tanaka, M. Kotsugi, K. Fukumoto, T. Ohkochi, T. Nakamura, T. Matsushita, T. Muro, M. Oura, Y. Senba, H. Ohashi, A. Kakizaki, C. Mitsumata, and T. Kinoshita, Phys. Rev. B **85**, 104418 (2012).
[33] G. van Der Laan, N. D. Telling, A. Potenza, S. S. Dhesi, and E. Arenholz, Phys. Rev. B **83**, 064409 (2011).
[34] O. Gomonay, T. Jungwirth, and J. Sinova, Phys. Rev. Lett. **117**, 017202 (2016).
[35] F. Kronast and S. V. Molina, J. Large-Scale Res. Facil. **2**, A90 (2016).
[36] S. Parkin and S.-H. Yang, Nat. Nanotechnol. **10**, 195 (2015).
[37] S. Selzer, U. Atxitia, U. Ritzmann, D. Hinzke, and U. Nowak, Phys. Rev. Lett. **117**, 107201 (2016).
[38] S. K. Kim, O. Tchernyshyov, and Y. Tserkovnyak, Phys. Rev. B **92**, 020402(R) (2015).
[39] Q. Shao *et al.*, Nat. Commun. **9**, 3612 (2018).
[40] O. Gomonay, S. Kondovych, and V. Loktev, J. Magn. Magn. Mater. **354**, 125 (2014).
[41] K. S. R. Menon, S. Mandal, J. Das, T. O. Menteş, M. A. Niño, A. Locatelli, and R. Belkhou, Phys. Rev. B **84**, 132402 (2011).
[42] L. Baldrati, C. Schneider, T. Niizeki, R. Ramos, J. Cramer, A. Ross, E. Saitoh, and M. Kläui, Phys. Rev. B **98**, 014409 (2018).
[43] I. Gray, T. Moriyama, N. Sivadas, G. M. Stiehl, J. T. Heron, R. Need, B. J. Kirby, D. H. Low, K. C. Nowack, D. G. Schlom, D. C. Ralph, T. Ono, and G. D. Fuchs, Phys. Rev. X **9**, 041016 (2019).